Journal of Innovative Optical Health Sciences
Vol. 2, No. 2 (2009) 179–187

World Scientific
www.worldscientific.com

A NEAR-INFRARED FLUORESCENT DEOXYGLUCOSE DERIVATIVE FOR OPTICAL IMAGING OF EXPERIMENTAL ARTHRITIS

XIUPING LIU*, ZHENGMING XIONG†, SHEEN-WOO LEE†,
JELENA LEVI†, SHAHRIAR YAGHOUBI†, SANDIP BISWAL†,
SANJIV SAM GAMBHIR† and ZHEN CHENG†,‡

*School of Life Science & Technology
Huazhong University of Science and Technology
Wuhan 430074, China

†Molecular Imaging Program at Stanford (MIPS)
Departments of Radiology and Bioengineering, Bio-X Program
Stanford University, California 94305, USA
‡zcheng@stanford.edu

The purpose of this study is to investigate whether a near-infrared fluorescence (NIRF) probe, Cy5.5-D-glucosamine (Cy5.5-2DG), can image arthritis in collagen-induced arthritic (CIA) mice. The presence of arthritis was verified by both visual examination and micro-computed tomography (MicroCT) imaging. CIA mice were imaged by a micro-positron emission tomography (MicroPET) scanner one hour after intravenous injection of 2-deoxy-2-[^{18}F]fluoro-D-glucose ([^{18}F]FDG). After radioactivity of [^{18}F]FDG decayed away, Cy5.5-2DG was injected into a lateral tail vein of the mice. Arthritic tissue targeting and retention of Cy5.5-2DG in CIA mice were evaluated and quantified by an optical imaging system. Inflammatory tissue in CIA mice was clearly visualized by [^{18}F]FDG-MicroPET scan. NIRF imaging of Cy5.5-2DG in the same mice revealed that the pattern of localization of Cy5.5-2DG in the arthritic tissue was very similar to that of [^{18}F]FDG. Quantification analysis further showed that [^{18}F]FDG uptake in arthritic tissues at one hour post-injection (p.i.) and Cy5.5-2DG uptakes at different time points p.i. were all well correlated (r^2 over 0.65). In conclusion, Cy5.5-DG can detect arthritic tissues in living mice. The good correlation between the [^{18}F]FDG uptake and Cy5.5-2DG accumulation in the same arthritic tissue warrants further investigation of Cy5.5-2DG as an approach for assessment of anti-inflammatory treatments.

Keywords: Near-infrared fluorescence; arthritis; fluorescent deoxyglucose; FDG.

1. Introduction

Molecular optical imaging of diseases has become an important component in biomedical research.[1–3] Because of the strong tissue penetration ability of light in the near-infrared (NIR) region (650–900 nm wavelength), NIR fluorescence (NIRF) imaging provides a powerful tool for non-invasively studying diseases at molecular level in preclinical animal models, and also has great potential for translation into clinical applications.[4–7] Optical imaging does not involve exposure to ionizing radiation. It is inexpensive, highly sensitive and allows high

‡Corresponding author.

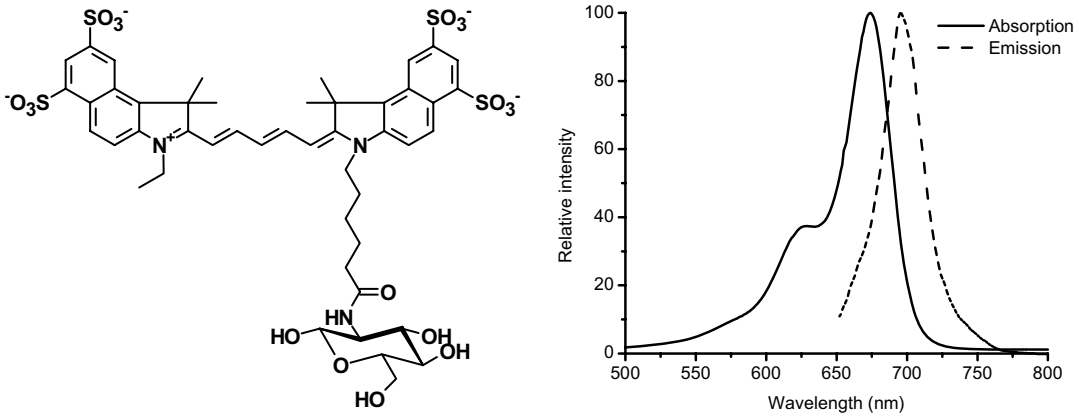

(a) (b)

Fig. 1. (a) Schematic structure of Cy5.5-2DG. (b) Absorption (675 nm) and emission fluorescence (695 nm) spectra of Cy5.5-2DG in water.

throughput screening since it requires short acquisition time to obtain a good image.[1,5] Recent advance in NIR optical imaging has demonstrated that it is a viable method for non-invasively monitoring disease states at the molecular level, localizing and staging diseases such as cancer, and even assessing the treatment efficacy of new therapeutic drugs.[8–11]

Rheumatoid arthritis (RA) is the most common rheumatic disease in humans and it represents a significant health problem.[12] Extensive basic science and clinical research has been devoted to finding successful treatments for RA. Early diagnosis, accurate staging, and timely monitoring of treatment response are expected to make significant contributions for effective RA management.[12] Since RA predominately affects the small joints of hands and feet, optical imaging techniques are considered suitable approaches for studying RA in these superficial hand joints in small animals.[13] Previous studies have demonstrated that NIR optical imaging can be used for detection of arthritis including RA by using different fluorescent probes.[14–21]

We reported recently that a NIR fluorescent glucose analog, Cy5.5 conjugated D-glucosamine (Cy5.5-2DG, its structure and absorption and emission spectra shown in Fig. 1), could target tumors specifically in cell culture and in mice.[22] Both human glioma U87MG and melanoma A375M can be clearly detected in mouse xenografts with Cy5.5-2DG. Good tumor/muscle contrast is obtained as early as 30 min p.i. of Cy5.5-2DG.[22] Here, we further investigate the possibility of imaging arthritic tissue *in vivo* using Cy5.5-2DG in a mouse model of collagen-induced arthritis. Multimodality small-animal imaging techniques including micro-computed tomography (MicroCT), micro-positron emission tomography (MicroPET), and NIRF imaging were used to rapidly assess the arthritic tissue targeting ability of Cy5.5-2DG.

2. Materials and Methods

2.1. *General aspects*

Cy5.5 monofunctional N-hydroxysuccinimide (NHS) ester (Cy5.5-NHS) was purchased from GE Healthcare Life Sciences (Piscataway, NJ). Bovine type II collagen dissolved at 2 mg/ml in 0.05 M Acetic Acid was purchased from Chondrex Inc. (Redmond, WA). All other reagents were obtained from Sigma-Aldrich Chemical Co. (St. Louis, MO). A Dionex Summit high-performance liquid chromatography (HPLC) system (Dionex Corporation, Sunnyvale, CA) equipped with a 170U 4-Channel UV-Vis absorbance detector was used for purification and analysis of Cy5.5 labeled compound. UV detection wavelengths were 218 nm, 280 nm and 590 nm for all the experiments. Both semi-preparative (Zorbax SB-C18, 9.4 mm × 250 mm, Agilent Technologies, Inc. Santa Clara, CA) and analytical (Dionex, Sunnyvale, CA. Acclaim 120 C18, 4.6 mm × 250 mm) reverse phase HPLC columns were used. The mobile phase was solvent A, 0.1% trifluoroacetic acid (TFA) in water and solvent B,

Abbreviations: NIRF, near-infrared fluorescence; Cy5.5-2DG, Cy5.5-D-glucosamine; [^{18}F]FDG, 2-deoxy-2-[^{18}F]fluoro-D-glucose; HPLC, high-performance liquid chromatography; PET, positron emission tomography; p.i., post-injection.

0.1% TFA in acetonitrile (CH_3CN). Matrix-assisted laser desorption/ionization time-of-flight mass spectrometry (MALDI-TOF-MS) was performed by the Stanford Protein and Nucleic Acid Biotechnology Facility, Stanford University. 2-deoxy-2-[^{18}F]fluoro-D-glucose ([^{18}F]FDG) was produced by cyclotron facility, Molecular Imaging Program at Stanford (Stanford, CA).

2.2. *Imaging probe Cy5.5-2DG*

Cy5.5-2DG was synthesized based on the method we reported before.[22] Briefly, D-Glucosamine (16.0 μmol in 34.5 μL H_2O) was conjugated with Cy5.5-NHS (1.60 μmol in 160 μL H_2O) in sodium phosphate buffer (Na_2HPO_4, pH = 9.0, 0.1 M, 805.5 μL). After overnight incubation at 4°C in the dark, the reaction was quenched by adding 100 μL of 1% TFA. The final product was purified by C-18 semi-preparative HPLC and confirmed by MALDI-TOF-MS. The maximum wavelengths of excitation and emission for Cy5.5-2DG were 675 nm (λ_{ab}) and 695 nm (λ_{em}), respectively (Fig. 1). The product was redissolved in saline at a concentration of 1 mg/mL, and stored in the dark at −80°C until use.

2.3. *Induction of collagen-induced arthritis in mice*

The mouse model of collagen-induced arthritis (CIA) is an experimental autoimmune disease induced by immunization with collagen type II. It shares several clinical, immunological and pathological features with human RA, therefore it is widely used in RA research.[23] All animal experiments were approved by the Stanford University Animal Research Internal Review Board. DBA1/J mice were purchased from Jackson Laboratories (Bar Harbor, ME). Complete Freund's Adjuvant (CFA), containing 2 mg/ml inactivated *M. tuberculosis,* and bovine type II collagen were mixed to produce a thick emulsion. Eight-to-ten weeks old DBA1/J mice were injected with 100 μl of the collagen/CFA emulsion subcutaneously 2 cm from the base of the tail. After 21 days, these mice were boosted subcutaneously with 100 μl of an emulsion containing equal volumes of Incomplete Freund's Adjuvant and collagen at the base of the tail. The incidence of inflammation was then synchronized by injecting 50 μg of lipopolysaccharide (LPS) intraperitoneally, three days after the boost. Within a week, 80–100% of the mice developed arthritis and paw inflammation.

2.4. *MicroCT imaging of mouse arthritis*

The mice were imaged with a microCT scanner (eXplore RS MicroCT System, GE Healthcare, Piscataway, NJ) to verify arthritis development after collagen induction. Mice were put on the microCT scanning gantry and scanned for 10 min at a voxel resolution of 45 microns. The image acquisition and reconstruction were done using GE built-in software (Evolver and eXplore Reconstruction Interface, GE Healthcare, Piscataway, NJ). The reconstructed images were viewed using GEMS Microview.

2.5. *[^{18}F]FDG-microPET imaging of inflammation in mice*

MicroPET imaging of arthritic mice was performed on a microPET R4 rodent model scanner (Concorde Microsystems Inc, Knoxville, TN). The mice were injected with 5.55 MBq (150 μCi) of [^{18}F]FDG through tail vein. At 1 h p.i., mice were anesthetized with 2% isoflurane, and placed in the prone position and near the center of the field of view of a microPET scanner. Five-minute static scans were obtained and images were reconstructed by a two-dimensional ordered subsets expectation maximum (OSEM) algorithm. Regions of interest (ROIs) were drawn over the joints or paws on decay-corrected whole-body coronal images. The maximum counts per pixel per minute were obtained from the ROI and converted to counts per milliliter per minute by using a calibration constant. By assuming a tissue density of 1 g/mL, the ROI values were converted to counts/g/min. An image ROI-derived percentage injected dose per gram of tissue (%ID/g) was then determined by dividing counts per gram per minute with injected dose.

2.6. *Optical imaging of mice inflammation*

After radioactivity of [^{18}F]FDG decayed away (overnight p.i.), the same group of mice was subjected to optical imaging. *In vivo* NIRF imaging was performed with an IVIS 200 small-animal imaging system (Xenogen, Alameda, CA). A Cy5.5 filter set was used for acquiring Cy5.5-2DG fluorescence. Identical illumination settings (lamp voltage, filters, f/stop, field of views, binning) were used to acquire all images, and fluorescence emission was normalized to photons per second per centimeter square per steradian (p/s/cm^2/sr). Images were

acquired and analyzed using Living Image 2.5 software (Xenogen, Alameda, CA). Mice with arthritis ($n = 3$) were injected via tail vein with 0.5 nmol Cy5.5-2DG and subjected to optical imaging at various time points p.i. All NIR fluorescent images were acquired using one-second exposure time (f/stop = 4) and displayed in the same scale of fluorescence intensity. For determining fluorescence intensity in arthritic tissues, maximum fluorescence intensities (p/s/cm^2/sr) of the paws or joints area were calculated by the region-of-interest (ROI) function of Living Image software integrated with Igor (Wavemetrics, Lake Oswego, OR).

2.7. *Statistical analysis*

Statistical analysis was performed using the Student's t-test for unpaired data. A 95% confidence level was chosen to determine the significance between groups, with $p < 0.05$ being significantly different.

3. Results

3.1. *MicroCT imaging of arthritis*

Five days after injection of LPS, the mice ($n = 3$) paws and knees were visually examined. Erythema and remarkable swelling of the paws and knees were clearly observed in all mice (Fig. 2(a)1–5), indicating severe RA-associated inflammation. The severity of the arthritis or joint inflammation of each paw and knee in the same mouse was different.

MicroCT imaging was then performed to verify the presence of RA in mice. The images shown in Fig. 2(b) are cross-sectional axial (Fig. (b)1), sagittal (Fig. (b)2) and coronal (Fig. (b)3) view of the right knee. Marginal bone erosion and joint space narrowing were identified by microCT imaging, which were solid evidences of arthritis. Furthermore, the anteroposterior view of the right front limb (Fig. 2(c)1) and lateral view of the right hind limb (Fig. 2(c)2) by maximum intensity projection of microCT data provided more evidence of arthritis. The microCT image of the right front limb (Fig. 2(c)1) showed (1) narrowed metacarpophalangeal and interphalangeal joint spaces; (2) marginal and central bone erosions; (3) periarticular osteopenia; (4) periosteal reaction along the radius, ulna, as well as metaphalangeal and phalangeal bones; and (5) pathologic fracture of the fifth metaphalangeal bone. The image of the right hind limb showed (1) narrowed knee joint space; (2) small and fused tarsal bones due to inflammation; and (3) periosteal reaction along the metatarsal and phalangeal bones. Overall, the anatomic changes and deformation of the joints clearly demonstrated the development of RA in the mice.

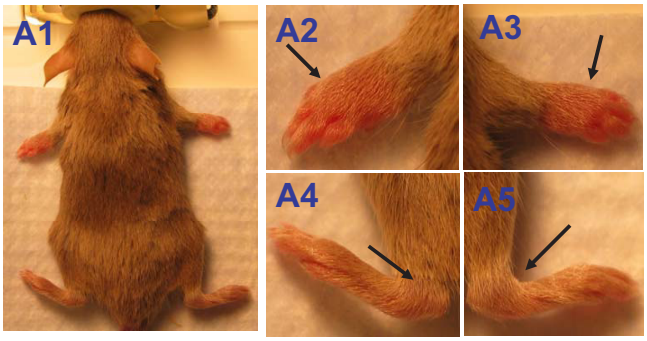

(a)

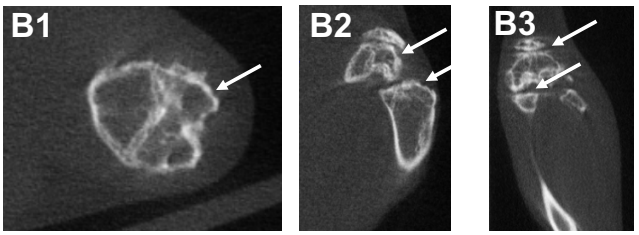

(b)

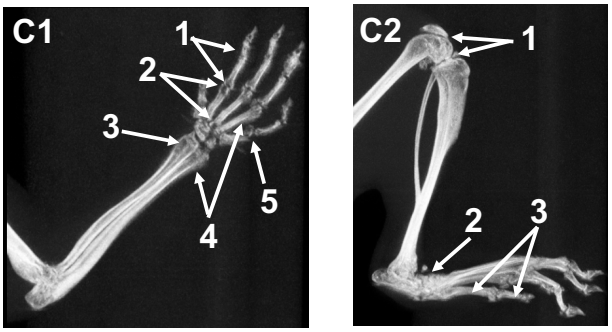

(c)

Fig. 2. (a) Photographs of a mouse with arthritic paws. ((a)1) whole-body photograph of the mouse; ((a)2) the front left paw of the mouse; ((a)3) the front right paw of the mouse; ((a)4) the hind left paw of the mouse; and ((a)5) the hind right paw of the mouse. Arrows point to the swelling inflamed paws and knees. (b) MicroCT visualization of right hind knee of the same mouse (slice thickness, 45 μm). These images show cross-sectional axial ((b)1), sagittal ((b)2) and coronal ((b)3) views of the knee. Arrows indicate marginal bone erosion and joint space narrowing. (c) Maximum intensity projection of microCT data. ((c)1) Anteroposterior view of the right front limb; and ((c)2) lateral view of the right hind limb. Arrows indicate anatomic changes caused by arthritis.

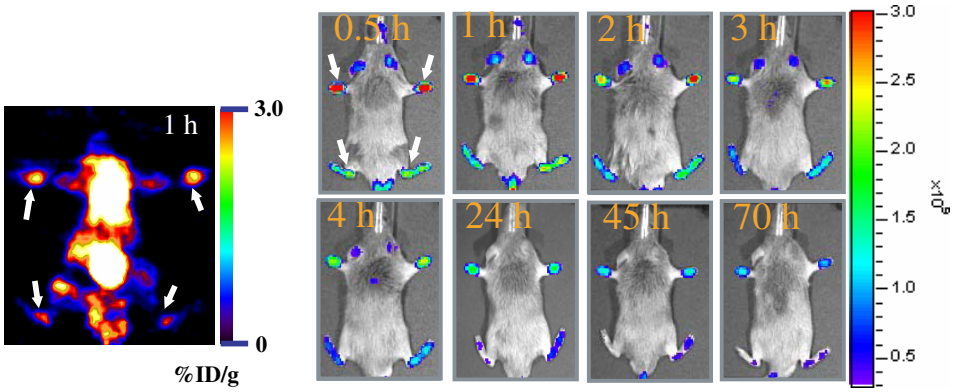

(a) (b)

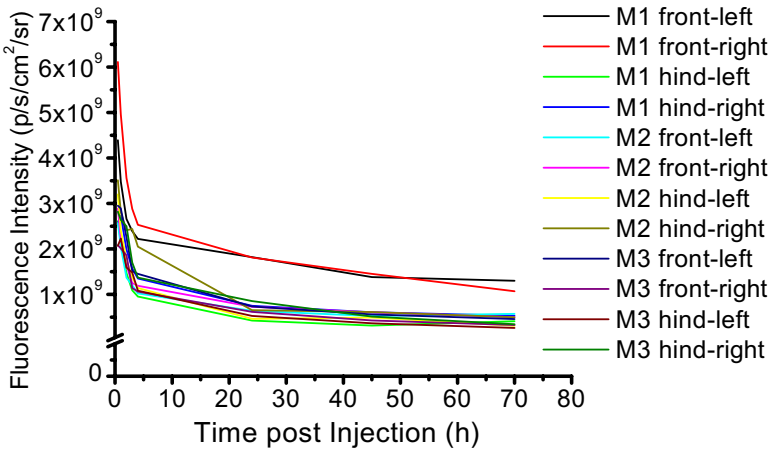

(c)

Fig. 3. (a) Decay corrected coronal [^{18}F]FDG-microPET image of the same DBA1/J mouse shown in the Fig. 2(a). PET images were acquired one hour after tail vein injection of (5.55 MBq, 150 μCi) [^{18}F]FDG. Arrows indicate the arthritic paws and joints. (b) *In vivo* fluorescence imaging of an arthritic mouse (the same mouse shown in Fig. 2(a)) after intravenous injection of 0.5 nmol Cy5.5-2DG. Fluorescence signal from probes is pseudo-colored red. (c) Time course of fluorescence intensities in each paw of mice [3 mice (M1, M2 and M3 represent mouse 1, 2 and 3, respectively), in 12 paws (front left, front right, hind left and hind right)] after Cy5.5-2DG injection. Fluorescence intensity was recorded as photons per second per centimeter square per steradian (p/s/cm^2/sr).

3.2. *[^{18}F]FDG-microPET imaging of inflammation*

Since the severity of the joint inflammation of each paw in the mice displayed substantial variation, [^{18}F]FDG-microPET scan was performed in order to visually identify the inflammation and evaluate the inflammation activity in each paw. The arthritic paws and joints were clearly visualized by PET imaging. Moreover, [^{18}F]FDG displayed different extent of accumulation in each paw and knee. Figure 3(a) clearly illustrates the observed variability in [^{18}F]FDG uptake. Both front paws showed much higher [^{18}F]FDG uptake than that of hind paws, suggesting different inflammation activity. Quantification of [^{18}F]FDG accumulation in all paws ($n = 12$) showed that the uptake ranged from 0.90 to 3.22%ID/g.

3.3. *Optical imaging of mice inflammation*

Whole-body optical imaging of the mice was then performed by using an IVIS200 system to monitor the accumulation of Cy5.5-2DG in paws with different grades of arthritis. A series of NIRF images of the same mouse imaged with [^{18}F]FDG are shown in Fig. 3(b). Cy5.5-2DG exhibited different levels of accumulation in each paw and knee from 30 min

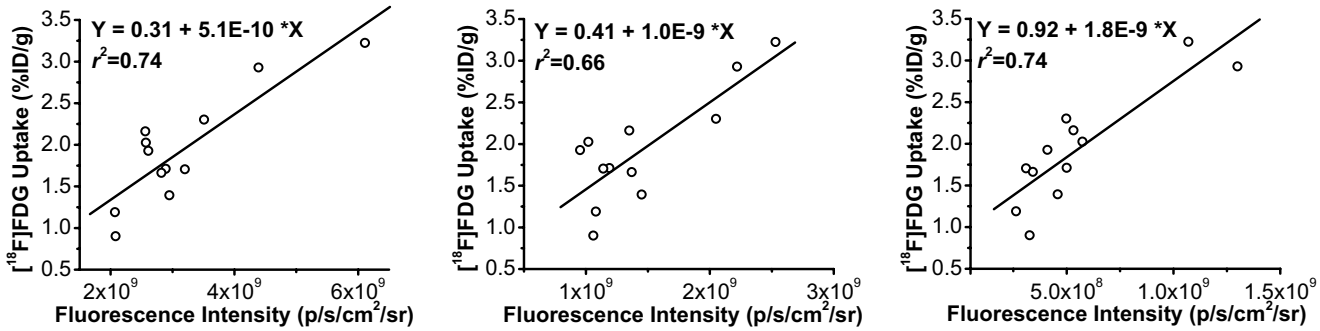

(a) (b) (c)

Fig. 4. Correlation of NIRF signal intensities in arthritic paws of three mice at different time points p.i. of Cy5.5-2DG ((a): 0.5 h, (b): 4 h; and (c): 70 h) and [^{18}F]FDG uptakes at 1 h p.i. [^{18}F]FDG uptake was determined from microPET images, expressed as %ID/g. NIRF signal intensity was expressed as maximum photons/cm^2/s/sr, obtained from ROIs drawn over the inflammation sites on the mice images. The correlations are $r^2 = 0.74$, 0.66 and 0.74 for (a), (b) and (c), respectively.

up to 70 h p.i. of 0.5 nmol of probe. Quantitative analysis of these images was performed, and the fluorescence intensities for Cy5.5-2DG in each paw as a function of time p.i. were depicted in Fig. 3(c). It was found that Cy5.5-2DG exhibited fast arthritic-tissue targeting characteristics *in vivo*. For all of the paws, the uptake of Cy5.5-2DG reached maximum within 1 h p.i. After 1 h p.i., the intensities of the signal slowly decreased, but over 10% of maximum signal intensities for all the paws still remained even after 70 h p.i. of the probe.

3.4. *Correlation between optical imaging and [^{18}F]FDG-microPET imaging*

To determine the relationship between [^{18}F]FDG and Cy5.5-2DG uptakes in the arthritic tissue, regression analysis was performed for the data obtained from two imaging modalities. Good correlations were seen between the NIRF signal intensities at all time points imaged and [^{18}F]FDG accumulations at 1 h p.i. (r^2 over 0.60 for all analyses). Figures 4(a)–(c) illustrate the correlation between [^{18}F]FDG uptakes at 1 h p.i. and Cy5.5-2DG uptakes at 0.5 h, 4 h, and 70 h pi, respectively. It was found that the higher uptake of [^{18}F]FDG, the higher NIRF intensities. These results clearly suggested that Cy5.5-2DG uptake in arthritic tissue was associated with the inflammation activity.

4. Discussion

With the wide recognition of the importance of molecular imaging, more and more scientists in different disciplines are using molecular imaging techniques to study a variety of diseases at molecular level. Development of novel probes for imaging specific biomarkers and molecular events and processes has become even more crucial and urgent. It is expected that development of new imaging probes will expand the application of molecular imaging in pre-clinical research and its translation into the practice of personalized medicine.

[^{18}F]FDG is the most widely-used PET tracer for imaging diseases, particularly for cancer and diseases associated with inflammation including RA.[24–27] Our research was geared toward developing NIR fluorescent glucose analogs for optical imaging of disease metabolism in living subjects. Cy5.5-2DG was synthesized and evaluated in both tumor cell culture and mice. The results show that Cy5.5-2DG has good mouse serum stability, high uptake and retention in the tumors. However, the uptake of Cy5.5-2DG in tumor cells does not seem to involve glucose transporters and the hexokinase pathway.[22] Although the mechanism responsible for the uptake of Cy5.5-2DG in tumor cells has not been elucidated yet, the great ability of Cy5.5-2DG for tumor NIRF imaging and the similarity of the molecular structure of the probe to that of [^{18}F]FDG has motivated us to investigate its application for imaging inflammation-associated diseases. Cy5.5-2DG was thus evaluated in an experimental CIA mice model.

Although the CIA model is highly reproducible, visual examination of the mice found that the severities of inflammation induced by collagen for each paw and knee were quite different, which is

consistent with results of previous literature.[28,29] Research on the understanding the pathogenesis of this model has been extensively performed and well-documented.[30] [^{18}F]FDG-microPET imaging of the mice ($n = 3$) further confirmed this finding. Generally, arthritic tissue with higher severity showed higher uptake of [^{18}F]FDG. This can be easily comprehended from the PET image (Fig. 3) and quantification analysis of those images. NIRF imaging of the same mice was performed. The patterns of localization of Cy5.5-2DG in the arthritic tissue are very similar to that of [^{18}F]FDG (Figs. 3(a) and 3(b)). Cy5.5-2DG can clearly differentiate tissues with different grades of arthritis. Most importantly, [^{18}F]FDG uptake in arthritic tissue at 1 h p.i. and Cy5.5-2DG uptakes at different time points p.i. are well correlated ($r^2 = 0.74$, 0.66, and 0.74 for 0.5 h, 4 h and 70 h p.i., respectively; Fig. 4). These results are important findings as they suggest several potential applications of Cy5.5-2DG. First, Cy5.5-2DG seems suitable for NIRF imaging of arthritic joints *in vivo*. Second, Cy5.5-2DG may serve as a NIRF surrogate agent of [^{18}F]FDG and be used as a powerful tool for monitoring treatment effects of anti-inflammatory therapy. Future studies are required to investigate whether this probe can be beneficial in assessing crucial parameters in RA management.

Several NIRF probes for arthritis imaging have been reported before. These probes were developed for imaging unique targets or extra- and intra-cellular processes associated with the development and progression of arthritis. Both Cy5.5-labeled antibody against F4/80 antigen presented on the macrophage surface[21] and NIR fluorophore-conjugated folate[17] have been reported for specific detection of macrophages in RA. Another promising strategy for early detection of arthritis is to image protease *in vivo* based on the protease-activated NIRF probes.[18,19] Cy5.5-Annexin V is also used for imaging drug-induced cell apoptosis in the arthritic joint.[31] The molecular targets for the NIR probes discussed above are all well defined. These imaging agents can be used to non-invasively evaluate the expression and distribution of their targets involved in diseases. Although Cy5.5-2DG shows promising results for arthritis imaging, several critical issues remain to be addressed: (1) Is the accumulation of Cy5.5-2DG in arthritic tissue specific? (2) What is the molecular target in inflammed tissues that Cy5.5-2DG is interacting with? and (3) Is the uptake of Cy5.5-2DG due to the characteristic physiological changes of RA such as increased number of capillaries, enhanced capillary perfusion and permeability? Further evaluation of Cy5.5-2DG in some other arthritis animal models may provide useful information to elucidate its targeting mechanism. Research is undergoing in our lab to answer these important questions. Overall, revealing the mechanism responsible for Cy5.5-2DG molecular recognition of RA will help to determine its practical utilization and clinical applicability.

NIRF dyes Cy5.5-NHS, indocyanine green (ICG) and a hydrophilic carbocyanine derivative (1,1′-*bis*-[4-sulfobutyl] indotricarbocyanine-5,5′-dicarboxylic acid diglucamide monosodium salt [SIDAG]) are also reported for detection of arthritic joints *in vivo*.[15,20] Cy5.5-NHS can bind covalently to serum proteins such as albumin. It can identify arthritic joints likely due to nonspecific deposition. Moreover, cultured macrophages actively phagocytose Cy5.5-NHS, which explains the long signal stability of Cy5.5-NHS fluorescence up to 72 h in mice.[15] Although Cy5.5-NHS has already been reported to detect arthritis, Cy5.5-2DG may show some advantages over Cy5.5-NHS. First, Cy5.5-2DG cannot bind plasma protein covalently because it lacks the *N*-hydroxy-succinimide ester reactive moiety. This may reduce its total non-specific binding with serum protein. Second, this study for the first time demonstrates the correlation of Cy5.5-2DG uptake and [^{18}F]FDG uptake, which has not been reported for any arthritis targeting NIRF probes. This unique property highlights the great potential of Cy5.5-2DG for imaging arthritis. It would also be interesting to explore 2DG coupled with other NIR dyes such as Cy7 with longer emission wavelengths. Such a probe may further expand the applications of the probe for arthritis optical imaging, because of its better tissue penetration ability.

5. Conclusion

The results presented in this article indicate that the NIRF glucose analog, Cy5.5-2DG, can detect arthritic paws in living mice. More importantly, the Cy5.5-2DG accumulation in arthritic tissues

correlates well with the [^{18}F]FDG uptake. Therefore Cy5.5-2DG imaging may offer an approach for assessment of anti-inflammatory treatments and for use in imaging guided therapy.

Acknowledgments

This work was supported, in part, by National Natural Science Foundation of China (Grant No. 90508003), National Cancer Institute (NCI) Small Animal Imaging Resource Program (SAIRP) Grant R24 CA93862, and NCI *In Vivo* Cellular Molecular Imaging Center (ICMIC) Grant P50 CA114747 (SSG).

References

1. Massoud, T. F. and Gambhir, S. S., "Molecular imaging in living subjects: Seeing fundamental biological processes in a new light," *Genes Dev.* **17**, 545–580 (2003).
2. Ntziachristos, V., "Fluorescence molecular imaging," *Annu. Rev. Biomed. Eng.* **8**, 1–33 (2006).
3. Contag, C. H. and Bachmann, M. H., "Advances in *in vivo* bioluminescence imaging of gene expression," *Annu. Rev. Biomed. Eng.* **4**, 235–260 (2002).
4. Sevick-Muraca, E. M., Houston, J. P. and Gurfinkel, M., "Fluorescence-enhanced, near infrared diagnostic imaging with contrast agents," *Curr. Opin. Chem. Biol.* **6**, 642–650 (2002).
5. Ntziachristos, V., Bremer, C. and Weissleder, R., "Fluorescence imaging with near-infrared light: New technological advances that enable *in vivo* molecular imaging," *Eur. Radiol.* **13**, 195–208 (2003).
6. Tung, C. H., "Fluorescent peptide probes for *in vivo* diagnostic imaging," *Biopolymers* **76**, 391–403 (2004).
7. Weissleder, R. and Mahmood, U., "Molecular imaging," *Radiology* **219**, 316–333 (2001).
8. Mahmood, U. and Weissleder, R., "Near-infrared optical imaging of proteases in cancer," *Mol. Cancer Ther.* **2**, 489–496 (2003).
9. Achilefu, S., "Lighting up tumors with receptor-specific optical molecular probes," *Technol. Cancer. Res. Treat.* **3**, 393–409 (2004).
10. Lin, J., Zhang, Z., Zeng, S. *et al.*, "TRAIL-induced apoptosis proceeding from caspase-3-dependent and independent pathways in distinct HeLa cells," *Biochem. Biophys. Res. Commun.* **346**, 1136–1141 (2006).
11. Contag, P. R., "Whole-animal cellular and molecular imaging to accelerate drug development," *Drug. Discov. Today* **7**, 555–562 (2002).
12. Bresnihan, B., "Pathogenesis of joint damage in rheumatoid arthritis," *J. Rheumatol.* **26**, 717–719 (1999).
13. Mayer-Kuckuk, P. and Boskey, A. L., "Molecular imaging promotes progress in orthopedic research," *Bone* **39**, 965–977 (2006).
14. Simon, G. H., Daldrup-Link, H. E., Kau, J., Metz, S., Schlegel, J., Piontek, G. *et al.*, "Optical imaging of experimental arthritis using allogeneic leukocytes labeled with a near-infrared fluorescent probe," *Eur. J. Nucl. Med. Mol. Imaging* **33**, 998–1006 (2006).
15. Fischer, T., Gemeinhardt, I., Wagner, S., Stieglitz, D. V., Schnorr, J., Hermann, K. G. *et al.*, "Assessment of unspecific near-infrared dyes in laser-induced fluorescence imaging of experimental arthritis," *Acad. Radiol.* **13**, 4–13 (2006).
16. Pogue, B. W., "Near-infrared characterization of disease via vascular permeability probes," *Acad. Radiol.* **13**, 1–3 (2006).
17. Chen, W. T., Mahmood, U., Weissleder, R. and Tung, C. H., "Arthritis imaging using a near-infrared fluorescence folate-targeted probe," *Arthritis Res. Ther.* **7**, R310–317 (2005).
18. Wunder, A., Tung, C. H., Muller-Ladner, U., Weissleder, R. and Mahmood, U., "*In vivo* imaging of protease activity in arthritis: A novel approach for monitoring treatment response," *Arthritis Rheum.* **50**, 2459–2465 (2004).
19. Lai, W. F., Chang, C. H., Tang, Y., Bronson, R. and Tung, C. H., "Early diagnosis of osteoarthritis using cathepsin B sensitive near-infrared fluorescent probes," *Osteoarthritis Cartilage* **12**, 239–244 (2004).
20. Hansch, A., Frey, O., Hilger, I., Sauner, D., Haas, M. and Schmidt, D. *et al.*, "Diagnosis of arthritis using near-infrared fluorochrome Cy5.5," *Invest. Radiol.* **39**, 626–632 (2004).
21. Hansch, A., Frey, O., Sauner, D., Hilger, I., Haas, M. and Malich, A. *et al.*, "*In vivo* imaging of experimental arthritis with near-infrared fluorescence," *Arthritis Rheum.* **50**, 961–967 (2004).
22. Cheng, Z., Levi, J., Xiong, Z., Gheysens, O., Keren, S. and Chen, X. *et al.*, "Near-infrared fluorescent deoxyglucose analogue for tumor optical imaging in cell culture and living mice," *Bioconjug. Chem.* **17**, 662–669 (2006).
23. Brand, D. D., Kang, A. H. and Rosloniec, E. F., "The mouse model of collagen-induced arthritis," *Methods Mol. Med.* **102**, 295–312 (2004).
24. Gambhir, S. S., "Molecular imaging of cancer with positron emission tomography," *Nat. Rev. Cancer* **2**, 683–693 (2002).
25. Mochizuki, T., Tsukamoto, E., Kuge, Y., Kanegae, K., Zhao, S., Hikosaka, K. *et al.*, "FDG uptake and glucose transporter subtype expressions in experimental tumor and inflammation models," *J. Nucl. Med.* **42**, 1551–1555 (2001).

26. Goerres, G. W., Forster, A., Uebelhart, D., Seifert, B., Treyer, V., Michel, B. *et al.*, "F-18 FDG whole-body PET for the assessment of disease activity in patients with rheumatoid arthritis," *Clin. Nucl. Med.* **31**, 386–390 (2006).
27. Beckers, C., Ribbens, C., Andre, B., Marcelis, S., Kaye, O., Mathy, L. *et al.*, "Assessment of disease activity in rheumatoid arthritis with ^{18}F-FDG PET," *J. Nucl. Med.* **45**, 956–964 (2004).
28. Courtenay, J. S., Dallman, M. J., Dayan, A. D., Martin, A. and Mosedale, B., "Immunisation against heterologous type II collagen induces arthritis in mice," *Nature* **283**, 666–668 (1980).
29. Metselaar, J. M., van den Berg, W. B., Holthuysen, A. E. *et al.*, "Liposomal targeting of glucocorticoids to synovial lining cells strongly increases therapeutic benefit in collagen type II arthritis," *Ann. Rheum. Dis.* **63**, 348–353 (2004).
30. Brand, D. D., Kang, A. H. and Rosloniec, E. F., "Immunopathogenesis of collagen arthritis," *Springer Semin. Immunopathol.* **25**, 3–18 (2003).
31. Wunder, A., Schellenberger, E., Mahmood, U., Bogdanov Jr., A., Muller-Ladner, U., Weissleder, R. *et al.*, "Methotrexate-induced accumulation of fluorescent annexin V in collagen-induced arthritis," *Mol. Imaging* **4**, 1–6 (2005).